Vietnam Journal of Catalysis and Adsorption
Tạp chí xúc tác và hấp phụ Việt Nam

http://jca.edu.vn

Synthesis of MOFs and application for NO_x treatment by adsorption process

Do Thanh Trung[1], Vuong Thanh Huyen[2], Vu Ngoc Toan[3], Le Minh Thang[1,*]

[1] *Department of Chemical Engineering, School of Chemistry and Life Sciences, Hanoi University of Science and Technology, 1 Dai Co Viet Road, Hanoi, Vietnam*
[2] *Leibniz Institute für Katalyse. e.V., Albert-Einstein-Straße 29A, 18059 Rostock, Germany*
[3] *Institute of New Technology, Academy of Military Science and Technology, 17 Hoang Sam, Ha Noi, Vietnam*
** Email: thang.leminh@hust.edu.vn*

ARTICLE INFO

Received: 30/03/2026
Accepted: 04/05/2026
Published: 30/06/2026

Keywords:
UiO-66-X; MOF-5; NOx; adsorption

ABSTRACT

Nitrogen oxides (NO_x) are a group of gases causing adverse effects on human health as well as the environment. In this work, metal organic frameworks UiO-66-X (X = NH_2, OH, NO_2) and MOF-5 were synthesized by using solvothermal/hydrothermal methods. The obtained materials were characterized by X-ray diffraction, BET specific surface area and elemental analysis by using the ICP–OES method. NO adsorption process at room temperature were monitored by using a micro-reactor set up connected to an online GC. The NO adsorption capacities of all materials were low, at less than 0.02 mmol/g. Therefore, these materials need to be improved in order to perform further studies.

Introduction

Since the world underwent the process of industrialization and modernization, industrial factories have grown continuously, and transportation methods have developed, but along with that comes the reality of air pollution in the world. Among them, nitrogen oxides (NO_x) are among the leading causes affecting air quality and human health. Therefore, measures to control and minimize their emissions are essential.

Many efforts have been dedicated, and various materials have been designed for NO_x treatments. The first method is reducing NO_x into nitrogen by using NH3 or urea with or without the help of catalysts. In the reduction of NOx with catalysts, the process is divided into four branches: (1) Direct NO_x decomposition; (2) Three-Way Catalysts-TWC; (3) Selective catalytic reduction using hydrocarbons/ Hydrocarbon Selective Catalytic Reduction (HC - SCR); (4) Ammonia Selective Catalytic Reduction (NH3 - SCR) [1, 2]. One of the representatives for this process is vanadium-based materials [3-5]. Although these materials have various advantages such as high efficiency, wide-temperature activity, and low production cost [6, 7] they are not effective in some conditions such as dynamite manufacturing factories, which contain high NO_x emission, leading to the waste of NO_x resources. As a result, adsorption can be applied to reduce the content of NO_x. This process only keeps the gas in the material without further chemical reactions. Then, NO_x is desorbed to reuse NO_x. One of the materials for this process is zeolite, where its efficiency is proven in several experiments [8, 9], and MOFs, which is our work as well as some other publications [10, 11].

Metal organic frameworks (MOFs) are a class of materials formed by the connection between metal ions and organic ligands. They possess a wide range of structures, functional groups, and pore sizes [12]. Moreover, with the large surface area, they are applied in many subjects such as catalysis, magnetism,

https://doi.org/10.62239/jca.2026.021

fluorescence, gas adsorption, and separation [13-16], etc. As of 2005, scientists reported more than 12000 structures of MOF in the Cambridge Structural Database (CSD), while for every 3.9 years on average, there is a two-fold increase in the number of 3D MOFs [17]. In recent years, the majority of intensive research has focused on their synthesis and studies of gas sorption properties for hydrogen/methane storage, carbon dioxide capture, gas separations, and catalysis [18, 19]. Furthermore, the effort to investigate the synthesis and test the physical and chemical properties of MOFs is increasing to achieve a better understanding of their usage for the above applications [20].

MOFs show a great capacity in terms of gas storage. For example, Ebrahim and Decoste prepared amino-functionalized UiO-66 (UiO-66-NH_2) in the round-bottom flask by mixing $ZrCl_4$ and the linker in DMF, and the result showed extraordinarily high NO_2 adsorption capacities of 20.3 and 31.2 mmol g^{-1}, respectively [21], [22-24]. This happens due to the strong Lewis acid-base interaction between -NH_2 group in the material and NO_2 molecule. Additionally, studies of NO_x adsorption by using in-situ methods are also conducted. For NO_2, Peterson *et al.* [25-30] studied IR aspect of NO_2 adsorption on UiO-66-NH_2. The result showed that in the Fourier Transform infrared (ATR IR), NO_2 interactions at the second binding units (SBU) cause the decrease in metal oxide bonds in the SBU, leading to the additional peaks in the range of 600– 425 cm^{-1}. Moreover, the diffuse reflectance infrared Fourier transform spectroscopy (DRIFTS) spectra illustrate that the exposure of NO_2 to UiO-66-NH_2 is responsible for the loss of the -OH group at 3675 cm^{-1}, and the appearance of the signal of diazonium salt at 2280 cm^{-1}. MOF-5 is also the material that has a large BET surface area [31] and adsorption performance [32]. However, there is no experimental data of the adsorption process of NO by using UiO-66-X and MOF-5.

The objective of the present work is to investigate the adsorption characteristics in NO_x gases - NO by using UiO-66-X (X = NH_2, OH, NO_2) and MOF-5. Strong Lewis acid–base interactions between the –NH_2 groups in UiO-66-NH_2 are responsible for its high NO_2 adsorption capacity, therefore, a similar effect may be expected for NO adsorption. Secondly, the adsorption of NO using UiO-66-X (X = NH_2, OH, NO_2) and MOF-5 materials has not yet been studied. NO was also chosen since NO content in exhaust gas is extremely high, 90 – 95%, according to EGCSA [33].

First, these materials were synthesized by using the solvothermal and hydrothermal method, then they underwent various characteristic tests, including X-ray diffraction, BET specific surface area, and elemental analysis. After that, studies of NO adsorption were conducted using a micro-reactor setup connected to an online GC. These studies reveal the adsorption abilities of NO on materials as well as the effect of ligands on the process.

Experimental

Chemical

Zirconium chloride ($ZrCl_4$), Terephthalic acid with substituted groups (X-BDC, X = NH_2, OH, NO_2, H), Dimethyl formamide (DMF) were purchased from Sigma Aldrich in the United States of America with purity > 99%. Absolute ethanol, zinc nitrate hexahydrate ($Zn(NO_3)_2.6H_2O$), chloroform ($CHCl_3$) were also purchased from Merck (Germany).

Synthesis of UiO-66-NH_2 and UiO-66-NO_2

The synthesis of UiO-66-NH_2 was carried out by using the previous report with modifications [34]. Specifically, 1.5089 g of $ZrCl_4$ was dissolved in 90 mL of DMF in a 200 mL beaker. Also, 1.5646 g of H_2N-H_2BDC was dissolved in the same amount of DMF in another beaker. Both were stirred until completely dissolved. Then, the solution of H_2N-H_2BDC was slowly poured into the solution of $ZrCl_4$ while being stirred at room temperature for 20 minutes. The resulting solution was transferred into glass bottle before undergoing the pre-heating process at 80 ^oC for 13 hours. After that, the temperature was increased to 100 ^oC and kept for 24h. The resulting solid was filtered, then washed in 100 mL ethanol for 5 days (ethanol was replaced every 24h) while soaked in glycerol bath at 60 ^oC. Finally, the solid was filtered, washed with ethanol, and dried in Schlenk system under vacuum for 12h at room temperature. UiO-66-NO_2 was synthesized analogously by replacing H_2N-H2BDC with the equivalent molar amounts of O_2N-H_2BDC.

Synthesis of UiO-66-OH

The synthesis of UiO-66-OH is also based on the reported procedure with modifications [35]. Specifically, zirconium chloride ($ZrCl_4$, 306.9 mg, 1.31 mmol), 2-hydroxyterephthalic acid (218.6 mg, 1.20 mmol), and formic acid (4 mL) were dissolved in 30 mL of DMF in a beaker and ultrasonicated for 30 mins. The mixture was then transferred to an autoclave lined with polytetrafluoroethylene, sealed, placed in a preheated oven, and heated to crystallize at 130 **℃** for 13.5 h. After cooling to room temperature, the solid formed was then

filtered, washed several times with DMF, and then exchanged with ethanol for 4h to remove DMF. Finally, the solid was dried under vacuum at 60 ℃ for 4 h in a Schlenk system and then dried in an oven at 80 ℃ overnight to obtain UiO-66-OH powder.

Synthesis of MOF-5

The synthesis of MOF-5 is based on the previous work with modification [36]. Briefly, $Zn(NO_3)_2{\cdot}6H_2O$ (3.57 g, 12 mmol) and BDC (0.665 g, 4 mmol) were dissolved in 100 mL of dimethylformamide (DMF) and stirred for 3 min at room temperature. Then, the reaction mixture was transferred to an autoclave and heated in an oven at 120 ^oC for 24 h. After 24 h, the precipitate was redispersed in chloroform (100 mL) and stirred for 24 h for solvent exchange purposes. Finally, the precipitate was separated and heated at 100 ℃ in a dryer to evacuate the remaining trapped solvent.

Characterization

Powder X-ray diffraction (PXRD)

PXRD patterns of all samples were recorded on a Panalytical X'Pert PRO diffractometer equipped with an X'Celerator RTMS detector using Ni-filtered Cu-Kα radiation (λ = 0.154 nm) operating at 40 kV and 40 mA and a D8 Advance Bruker device using Cu-Kα radiation. Data were collected stepwise (0.021°/s) in the range of 5- 80º (2 theta) with a divergence slit of 2°. Peak positions and profiles were fitted with Pseudo-Voigt functions using the Highscore Plus software package (Panalytical). Phase identification was performed using the PDF-2 database of the International Center for Diffraction Data (ICDD).

Specific surface area

Brunauer-Emmett-Teller (BET) surface area, pore volume, and average pore diameter measurements were carried out by N_2 adsorption at 77 K using a Micromeritics ASAP 2010 instrument. Typically, 100 mg of sample was placed in the analysis tube and degassed at 200 ^oC for 4 h prior to exposure to N_2 gas.

Elemental analysis

The chemical composition of the catalysts was measured by inductively coupled plasma optical emission spectrometry (ICP-OES). The ICP-OES was performed using Varian 715-ES ICP-Emission-Spectrometer (Germany). Approximately 10 mg of the sample was mixed with 8 ml of aqua regia and 2 ml of hydrofluoric acid. The digestion was performed in a microwave-assisted sample preparation system "Multiwave 5000" from Anton Paar at ~ 220 ^oC and ~ 50 bar pressure. The digested solution was diluted up to 100 ml and measured with ICP-OES. The data analysis was performed on the Varian 715-ES software "ICP Expert". The content of zirconium was calculated by dividing the amount of zirconium in each sample by the mass of corresponding materials in the experiment.

Measurement of Adsorption Capacity

The initial sample was pretreated to remove water vapor and adsorbed gases in the sample. Briefly, about 0.10 grams of material was placed into the reaction column and fixed by glass wool. Then, the sample was heated to 200 ^oC at a rate of 15 ^oC /min. Simultaneously, a 99.999% N_2 was purged at a flow rate of 50 mL/min through the tube containing the material to remove impurities. After that, the temperature was kept at 200 ℃ for 1 hour before cooling down to room temperature.

Adsorption process

0.5% NO/Ar gas mixture was purged through the tube containing activated material at a flow rate of 20 - 35 mL/min. The output gas (NO) was detected by a UV multi-gas sensor detector (ABB gas Analyzer models AO-2020, Limas 21HW, Mannheim, Germany), and the concentration values were displayed and recorded every 15 seconds until the gas concentration remained constant.

Desorption process

The tested sample was heated to 200 ^oC at a rate of 5 ^oC/min under N_2 flow from 18 - 36 mL/min. The output gas (NO) was detected by a UV multi-gas sensor detector (ABB gas Analyzer models AO-2020, Limas 21HW, Mannheim, Germany). The NO concentration was measured and recorded every 15 seconds until the gas concentration remained unchanged.

Adsorbed Quantity (A_{ads}) was calculated as:

$$A_{ads} = \frac{Q_{out} \times S_{ads} \times 10^{-6}}{22.4 \times m}, mmol/g \quad (1)$$

$$S_{ads} = \sum_{0}^{t} \left[\frac{1}{2} \times (2C_{max} - (C_i + C_{i+1})) \times \Delta t\right) \quad (2)$$

Desorbed Quantity (A_{des}) was calculated as:

$$A_{des} = \frac{Q_{out} \times S_{des} \times 10^{-6}}{22.4 \times m}, mmol/g \quad (3)$$

$$S_{des} = \sum_{0}^{t} \left[\frac{1}{2} \times \left(C_j + C_{j+1} - 2C_{min}\right) \times \Delta t\right) \quad (4)$$

Where:

https://doi.org/10.62239/jca.2026.021

Q_{out}: Flow rate (ml/min) of the 0.5% NO/Ar flow in the adsorption process and the Ar flow in the desorption process

S_{ads}: Area formed by the vertical axis, horizontal axis, and adsorption process graph in adsorption process (ppm.min)

S_{des}: Area formed by the vertical axis, horizontal axis, and desorption process graph in desorption process (ppm. min)

C_{max}: Initial NO concentration (ppm)

C_{min}: Final NO concentration of measurement (ppm)

C_i: NO concentration at time *i* in the adsorption process (ppm)

C_j: NO concentration at time *j* in the desorption process (ppm)

Δt: Time between 2 measurements (minutes)

m: Mass of catalyst (grams)

Results and discussion

Powder X-ray diffraction (PXRD)

PXRD patterns of all three UiO-66 materials exhibit three characteristic diffraction peaks at 2θ = 7.4°, 8.6°, and 25.8°, corresponding to the (110), (200), and (600) planes (Fig. 1). Moreover, the remaining peaks are similar, in which UiO-66-NO_2 and UiO-66-OH have the weakest and the strongest intensity, respectively. Simultaneously, these sharp peaks with high intensity show that the highest crystallinity belongs to UiO-66-OH, whereas UiO-66-NO_2 is opposite. These data match the data from the reported literatures, proving the success of the synthesis [34, 35].

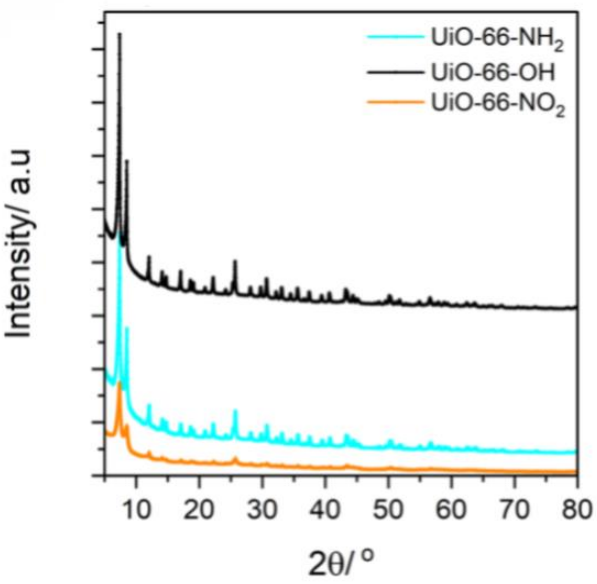

Fig. 1. XRD patterns of UiO-66-X (X = NH_2, OH, NO_2) samples.

All 2θ peaks were consistent with the synthesized UiO-66 parent materials, [37] each of which contains an inner $Zr_6O_4(OH)_4$ core. μ_3-O and μ_3-OH groups occupy the triangular faces of the Zr_6 octahedron. All the polyhedron edges are linked by the carboxylates (μ_2-(CO_2)) originating from X-BDC (X = NH_2, OH, NO_2) ligands, which leads to the formation of the $Zr_6O_4(OH)_4(CO_2)_{12}$ cluster. As a result, each Zr atom is eight-coordinated with a square antiprismatic coordination geometry with all ligands being bonded via oxygen atoms. One square face of the square antiprism is formed by oxygen atoms provided by carboxylates, whereas oxygen atoms from μ_3-O and μ_3-OH groups form the second square [38].

Standard MOF-5 contains four main peaks at 2θ = 6.8°, 9.6°, 13.7°, and 15.4°. However, this synthesized MOF-5 sample only contains two peaks at 2θ = 9.6°, and 15.4°, indicating the low crystallinity of the material (Fig. 2). On the other hand, the appearance of impurities can be clearly seen in the XRD pattern, which might belong to $Zn_x(OH)_y(NO_3)_z.tH_2O$ and their derivatives such as $Zn_5(OH)_8(NO_3)_2.2H_2O$ and $Zn_2(OH)_3NO_3$ [39]. Therefore, the synthesis did not meet the expectations compared to previous work [40].

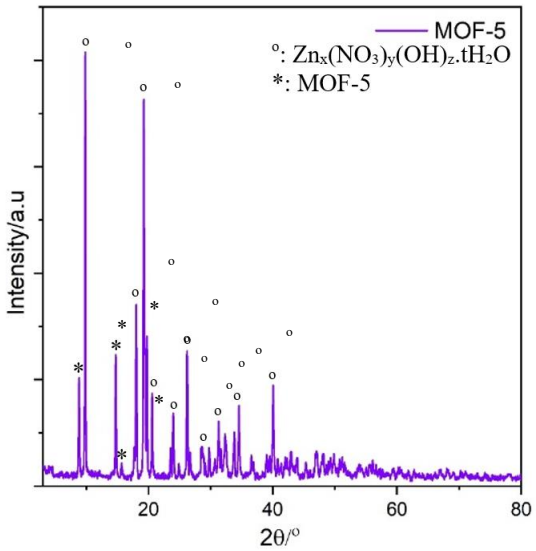

Fig. 2. XRD diagram of MOF-5.

Specific surface area

The BET surface area and pore volumes derived from the N_2 isotherms at 77K of three UiO-66-X samples. are listed in Table 1. The Brunauner – Emmett – Teller (BET) specific surface area of UiO-66-NH_2 is the largest at 1231.1 m^2/g, whereas that of UiO-66- NO_2 is the lowest at 552.5 m^2/g, and the pore volume for these two are 0.522cm^3/g and 0.225 cm^3/g, respectively, which are close to the reported results [34].

https://doi.org/10.62239/jca.2026.021

For MOF-5, the BET surface area is the lowest at only 15.2 m^2/g, whereas its pore volume is only 0.0384 cm^3/g. These numbers are far away from that of the reported work [31]. This happens due to the large amount of impurities in the material, which is verified in the XRD pattern (Fig. 2).

Table 1: Characteristic properties of all MOFs.

Material	S_{BET} (m^2/g)	Pore volume (cm^3/g)	Average %wt of Zr	Pore width (nm)
UiO-66-NH_2	1231.1	0.522	25.28	49.66, 1.74
UiO-66-OH	890.9	0.377	27.71	48,26, 1.74
UiO-66-NO_2	552.5	0.225	22.68	46.66, 1.74
MOF-5	15.2	0.038	-	1.71

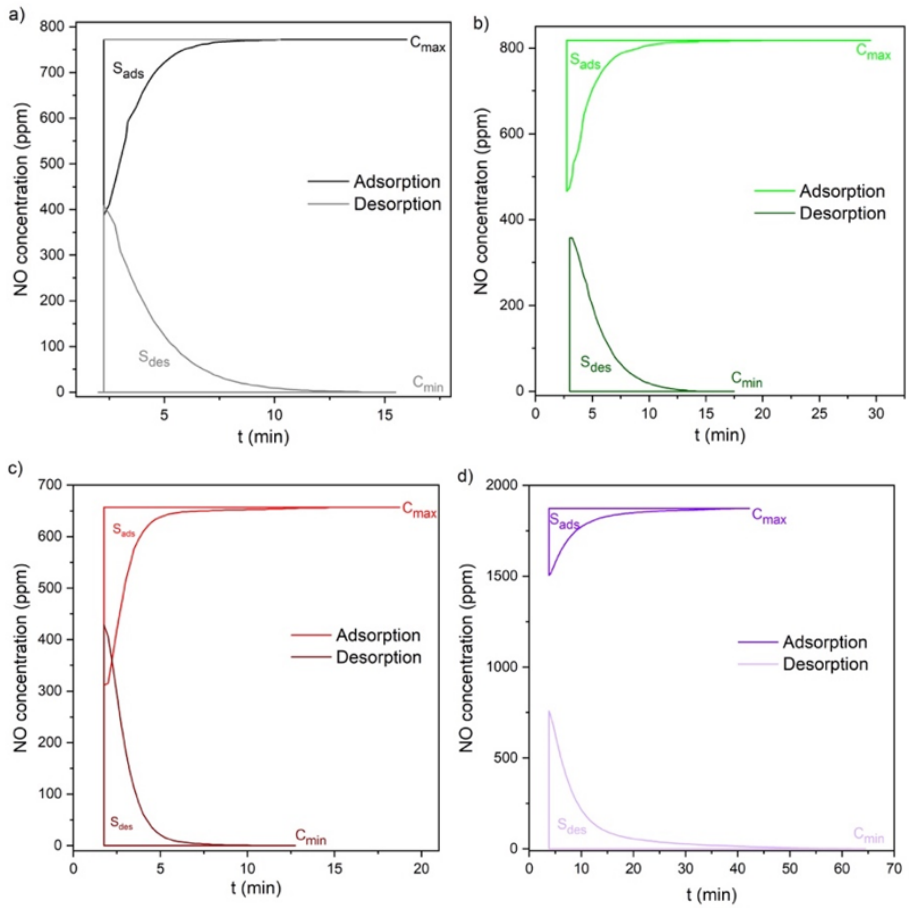

Fig. 3. Adsorption curves of NO in a) UiO-66-NH_2, b) UiO-66-OH, c) UiO-66-NO_2, and d) MOF-5.

Table 2: NO adsorption and desorption quantity measured by NO adsorption-desorption experiments in the microreactor setup.

Sample	Adsorption gas flow rate (mL/min)	Quantity NO adsorption (mmol/g)	Desorption gas flow rate (mL/min)	Quantity NO desorption (mmol/g)
UiO-66-NH_2	27.81	0.0071	22.54	0.0093
UiO-66-OH	20.52	0.0071	18.50	0.0083
UiO-66-NO_2	34.61	0.0078	36.24	0.0095
MOF-5	20.52	0.0186	20.52	0.0410

https://doi.org/10.62239/jca.2026.021

Elemental analysis

The Zr metal composition of the samples was determined by ICP-OES instrument. The results are also shown in Table 1. The theoretical zirconium content of UiO-66-NH_2, UiO-66-OH, and UiO-66-NO_2 is 31.2%, 31.09%, and 28.3%, respectively. However, the actual zirconium mass proportion of all UiO-66-X samples is much lower, indicating that impurities such as free ligands, and solvent molecules are still present in the materials with large quantities.3

NO adsorption

The adsorption curves of all materials obtained from the adsorption experiment in a microreactor set are depicted in Fig. 3. The calculated adsorption results are summarized in Table 2, where the amount of material used for the experiment was 0.099g for UiO-66-NH_2 and UiO-66-OH, 0.103g for MOF-5 and 0.098g for UiO-66-NO_2. The flow rate was 20.52 mL/min for UiO-66-OH and MOF-5, 27.84 mL/min for UiO-66-NH_2, and 34.61 mL/min for UiO-66-NO_2 during the adsorption process. , For the desorption process, the flow rates were 22.54 mL/min for UiO-66-NH_2, 18.50 mL/min for UiO-66-OH, 36.24 mL/min for UiO-66-NO_2, and 20.52 mL/min for MOF-5. The results show that MOF-5 has the highest NO adsorption capacity, whereas the lowest belongs to UiO-66-OH and UiO-66-NH_2, which is 0.0071 mmol/g. Compare it to other materials such as HKUST-1 with 9.0 mmol/g [41], Fe-MIL-88 with 2.5 mmol/g [42] and Fe_2(dobdc) with 6.2 mmol/g [43], these numbers are inconsiderable maybe due to incomparable adsorption conditions. Although MOF-5 contains impurities and possesses the lowest surface area but its higher NO adsorption capacity shows that NO adsorption in MOF-5 may be influenced by the participation of impurities, which have more affinity to NO and the pore size of MOF-5, which is the smallest in the studied samples (Table 1) but is also closer to kinetic diameter of the NO molecules (0.344 nm) [44]. Most notably, the adsorption quantity of all adsorbents is extremely low, meaning these materials are not yet suitable for NO storage.

However, the desorption quantity for all materials is higher than the adsorption quantity, which indicates that NO is desorbed easily at 200 ℃ and ligands from the MOF may also decompose to emit NO. It also suggests that there is the interaction between NO and the materials is the weak interaction. Therefore, the NO adsorption processes of MOFs should be studied further and improved.

Conclusion

In this work, UiO-66-NH_2, UiO-66-OH and UiO-66-NO_2 were successfully synthesized by using the solvothermal method. However, MOF-5 has not been succcesully synthesized, a large amount of impurities still present in the sample.

PXRD patterns demonstrate that all materials in the UiO-66-X group have similar main peaks, while those of MOF-5 shows various impurities. For the BET specific surface area, UiO-66-NO_2 has the lowest, whereas UiO-66-NH_2 has the highest in UiO-66-X group. On the contrary, BET surface area of MOF-5 is extremely low due to the appearance of several impurities. In the elemental analysis, the zirconium content in all materials is lower than the theoretical amount. Furthermore, the NO adsorption capacities of all materials are low, with less than 0.02 mmol/g. Meanwhile, the NO desorption quantity is higher than the adsorption, showing that NO is desorbed easily at the experimental conditions. However, this study only reveals a small part of NO adsorption by using the mentioned materials. Therefore, in order to gain deeper understanding, more studies have to be performed in the future.

Acknowledgments

This research has been supported by Project "Research on identifying cleaner production processes to Control and minimize environmental pollution risks for chemical-explosive materials factories in the military" (Code: 2023.85.54).

The authors acknowledge the facilities, the scientific and technical assistance at GeViCat Laboratory/Hanoi University of Science and Economic Cooperation and Development (BMZ) inside the framework "SDG Bilateral Graduate school program".

References

1. P. Granger, V.I. Parvulescu, Chem. Rev., 111(5) (2011) 3155-3207. https://doi.org/10.1021/cr100168g
2. M. Zhu, J.-K. Lai, U. Tumuluri, M.E. Ford, Z. Wu, I.E. Wachs, ACS Catal., 7(12) (2017) 8358-8361. https://doi.org/10.1021/acscatal.7b03149
3. P. Zhang, D. Li, Catal. Lett., 144(5) (2014) 959-963. https://doi.org/10.1007/s10562-014-1203-y
4. X. Zhao, et al., Appl. Catal. B: Environ., 183 (2016) 269-281. https://doi.org/10.1016/j.apcatb.2015.10.052
5. B. Guan, H. Lin, L. Zhu, B. Tian, Z. Huang, Chem. Eng. J., 181-182 (2012) 307-322. https://doi.org/10.1016/j.cej.2011.11.083

6. B. Ye, et al., Nano Convergence, 9(1) (2022) 51. https://doi.org/10.1186/s40580-022-00341-7
7. J. Xu, G. Chen, F. Guo, J. Xie, Chem. Eng. J., 353 (2018) 507-518. https://doi.org/10.1016/j.cej.2018.05.047
8. Q.-H. Trinh, S.H. Kim, Y.S. Mok, Chem. Eng. J., 302 (2016) 12-22. https://doi.org/10.1016/j.cej.2016.05.030
9. J. Yang, et al., J. Hazard. Mater., 162(2-3) (2009) 866-873. https://doi.org/10.1016/j.jhazmat.2008.05.111
10. M. Sun, A. Hanif, T. Wang, Q. Gu, J. Shang, Sep. Purif. Technol., 314 (2023) 123563. https://doi.org/10.1016/j.seppur.2023.123563
11. S. Shang, et al., Chem. Eng. J., 477 (2023) 147255. https://doi.org/10.1016/j.cej.2023.147255
12. H. Chae, D.Y. Siberio-Perez, J. Kim, Y. Go, M. Eddaoudi, A.J. Matzger, M. O'Keeffe, O.M. Yaghi, Nature, 427 (2004) 523. https://doi.org/10.1038/nature02311
13. X. Zhou, Y. Zhang, X. Yang, L. Zhao, G. Wang, J. Mol. Catal. A: Chem., 361 (2012) 12-16. https://doi.org/10.1016/j.molcata.2012.04.008
14. C.A. Kent, et al., J. Mater. Chem. A, 1(47) (2013) 14982-14989. https://doi.org/10.1039/C3TA14009A
15. A.S. Munn, G.J. Clarkson, F. Millange, Y. Dumont, R.I. Walton, CrystEngComm, 15(45) (2013) 9679-9687. https://doi.org/10.1039/C3CE41268G
16. H.C. Yoon, et al., Korean J. Chem. Eng., 32(12) (2015) 2501-2506. https://doi.org/10.1007/s11814-015-0088-9
17. N.W. Ockwig, O. Delgado-Friedrichs, M. O'Keeffe, O.M. Yaghi, Acc. Chem. Res., 38(3) (2005) 176-182. https://doi.org/10.1021/ar020022l
18. U. Müller, M. Schubert, F. Teich, H. Puetter, K. Schierle-Arndt, J. Pastré, J. Mater. Chem., 16(7) (2006) 626-636. https://doi.org/10.1039/B511962F
19. D.J. Collins, H.-C. Zhou, J. Mater. Chem., 17(30) (2007) 3154-3160. https://doi.org/10.1039/B702858J
20. S. Kitagawa, R. Kitaura, S.-i. Noro, Angew. Chem. Int. Ed., 43(18) (2004) 2334-2375. https://doi.org/10.1002/anie.200300610
21. I. Ahmed, S.H. Jhung, J. Hazard. Mater., 301 (2016) 259-276. https://doi.org/10.1016/j.jhazmat.2015.08.045
22. M.J. Ingleson, R. Heck, J.A. Gould, M.J. Rosseinsky, Inorg. Chem., 48(21) (2009) 9986-9988. https://doi.org/10.1021/ic9015977
23. A.H. Khan, K. Peikert, F. Hoffmann, M. Fröba, M. Bertmer, J. Phys. Chem. C, 123(7) (2019) 4299-4307. https://doi.org/10.1021/acs.jpcc.8b11919
24. A.M. Ebrahim, B. Levasseur, T.J. Bandosz, Langmuir, 29(1) (2013) 168-174. https://doi.org/10.1021/la302869m
25. B. Levasseur, C. Petit, T.J. Bandosz, ACS Appl. Mater. Interfaces, 2(12) (2010) 3606-3613. https://doi.org/10.1021/am100790v
26. A.M. Ebrahim, T.J. Bandosz, Microporous Mesoporous Mater., 188 (2014) 149-162. https://doi.org/10.1016/j.micromeso.2014.01.009
27. G.W. Peterson, J.J. Mahle, J.B. DeCoste, W.O. Gordon, J.A. Rossin, Angew. Chem., 128(21) (2016) 6343-6346. https://doi.org/10.1002/ange.201601782
28. X. Zhang, et al., J. Am. Chem. Soc., 139(45) (2017) 16289-16296. https://doi.org/10.1021/jacs.7b08748
29. X. Han, S. Yang, M. Schröder, Nat. Rev. Chem., 3(2) (2019) 108-118. https://doi.org/10.1038/s41570-019-0073-7
30. M. Bertmer, Annu. Rep. NMR Spectrosc., 101 (2020) 1-64. https://doi.org/10.1016/bs.arnmr.2020.07.003
31. A.M.P. Peedikakkal, I.H. Aljundi, Appl. Sci., 11(24) (2021) 11687. https://doi.org/10.3390/app112411687
32. D. Saha, Z. Bao, F. Jia, S. Deng, Environ. Sci. Technol., 44(5) (2010) 1820-1826. https://doi.org/10.1021/es9032309
33. EGCSA,. How are overboard nitrate emissions monitored?. https://www.egcsa.com/technical-reference/how-are-overboard-nitrate-emissions-monitored/ (accessed 12 June 2026).
34. M. Kandiah, et al., Chem. Mater., 22(24) (2010) 6632-6640. https://doi.org/10.1021/cm102601v
35. P. Li, et al., Chem. Bio. Eng., 2(1) (2025) 23-34. https://doi.org/10.1021/cbe.4c00108
36. H. Li, M. Eddaoudi, M. O'Keeffe, O.M. Yaghi, Nature, 402(6759) (1999) 276-279. https://doi.org/10.1038/46248
37. P. Kanoo, K.L. Gurunatha, T.K. Maji, J. Mater. Chem., 20(7) (2010) 1322-1331. https://doi.org/10.1039/B917029D
38. J.H. Cavka, et al., J. Am. Chem. Soc., 130(42) (2008) 13850-13851. https://doi.org/10.1021/ja8057953
39. T. Ramesh, T. Madhu, Int. J. Inorg. Chem., 2015 (2015) 1-11. https://doi.org/10.1155/2015/536470
40. J. Li, S. Cheng, Q. Zhao, P. Long, J. Dong, Int. J. Hydrogen Energy, 34 (2008) 1-6. https://doi.org/10.1016/j.ijhydene.2008.11.048
41. B. Xiao, et al., J. Am. Chem. Soc., 129(5) (2007) 1203-1209. https://doi.org/10.1021/ja066098k
42. J. Eubank, S. Wuttke, B. Xiao, P. Wheatley, P. Bazin, J.-C. Lavalley, M. Daturi, A. Vimont, G. De Weireld, Chem. Mater., 25(9) (2013) 1592-1599. https://doi.org/10.1021/cm304037x
43. E.D. Bloch, W.L. Queen, S. Chavan, P.S. Wheatley, J.M. Zadrozny, R. Morris, C.M. Brown, C. Lamberti, S. Bordiga, J.R. Long, J. Am. Chem. Soc., 137(10) (2015) 3466-3469. https://doi.org/10.1021/ja5132243
44. A. Alzhrani, C.J. Jameson, S. Murad, Ind. Eng. Chem. Res., 65(5) (2026) 2892-2909. https://doi.org/10.1021/acs.iecr.5c04316